Nuclear Engineering and Technology 51 (2019) 1540–1553

Contents lists available at ScienceDirect

Nuclear Engineering and Technology

journal homepage: www.elsevier.com/locate/net

Original Article

System dynamics simulation of the thermal dynamic processes in nuclear power plants

Mohamed El-Sefy [a, *], Mohamed Ezzeldin [a], Wael El-Dakhakhni [a], Lydell Wiebe [a], Shinya Nagasaki [b]

[a] Department of Civil Engineering, CaNRisk NSERC-CREATE Program on Canadian Nuclear Energy Infrastructure Resilience Under Systemic Risks, McMaster University, Hamilton, ON, L8S 4L7, Canada
[b] Department of Engineering Physics, CaNRisk NSERC-CREATE Program on Canadian Nuclear Energy Infrastructure Resilience Under Systemic Risks, Canada Research Chair in Nuclear Fuel Cycle and Radioactive Waste Management, McMaster University, Hamilton, ON, L8S 4L7, Canada

ARTICLE INFO

Article history:
Received 27 November 2018
Received in revised form
17 April 2019
Accepted 19 April 2019
Available online 20 April 2019

Keywords:
Nuclear power plant
Pressurized water reactor
Dynamic probabilistic risk assessment
System dynamics
Systemic risk
Thermal dynamic processes

ABSTRACT

A nuclear power plant (NPP) is a highly complex system-of-systems as manifested through its internal systems interdependence. The negative impact of such interdependence was demonstrated through the 2011 Fukushima Daiichi nuclear disaster. As such, there is a critical need for new strategies to overcome the limitations of current risk assessment techniques (e.g. the use of *static* event and fault tree schemes), particularly through simulation of the nonlinear *dynamic* feedback mechanisms between the different NPP systems/components. As the first and key step towards developing an integrated NPP dynamic probabilistic risk assessment platform that can account for such feedback mechanisms, the current study adopts a system dynamics simulation approach to model the thermal dynamic processes in: the reactor core; the secondary coolant system; and the pressurized water reactor. The reactor core and secondary coolant system parameters used to develop system dynamics models are based on those of the Palo Verde Nuclear Generating Station. These three system dynamics models are subsequently validated, using results from published work, under different system perturbations including the change in reactivity, the steam valve coefficient, the primary coolant flow, and others. Moving forward, the developed system dynamics models can be integrated with other interacting processes within a NPP to form the basis of a dynamic system-level (systemic) risk assessment tool.

1. Introduction

Nuclear power is considered a vital solution to the continuous demand for clean, secure, sustainable and reliable energy [1]. The 448 nuclear power reactor units currently operating around the world provide 10.4% of the global electricity [2], while a total of 60 and 168 units are currently undergoing their construction and planning stages, respectively [3]. As a result of their associated cost, nuclear power plants (NPP) are mega infrastructure projects that are expected to operate for a relatively long time span, whereas the plant design and planning decisions must account for abnormal events. Recent events (e.g. Fukushima Daiichi nuclear disaster) have highlighted that natural hazard intensity can exceed that originally used for plant design [4]. In addition to natural hazards, anthropogenic hazards (e.g. fire, internal flooding, and human-made errors) might also initiate events that lead to a component and/or system failure. In addition, both natural and anthropogenic hazards can, independently or through interaction, trigger cascade disasters (defined as disasters in which impacts progressively increase over time and cause unexpected secondary events of more significant consequences [5]) throughout a major part of or the entire NPP, due to component/system interdependence. Such disasters have been known to cause major failures in NPP (e.g. Three Mile Island accident in 1979, Chernobyl disaster in 1986, H.B. Robinson NPP fire event in 2010, and Fukushima Daiichi disaster in 2011), as described by Little [6], Mosleh [7], and Perrow [8]. NPP disasters can cause substantial economic and human losses where, for example, the Fukushima Daiichi disaster resulted in the release of a large amount of radioactive material [9], and more than 100,000 people were forced to evacuate communities within 25

* Corresponding author.
E-mail addresses: elsefym@mcmaster.ca (M. El-Sefy), ezzeldms@mcmaster.ca (M. Ezzeldin), eldak@mcmaster.ca (W. El-Dakhakhni), wiebel@mcmaster.ca (L. Wiebe), nagasas@mcmaster.ca (S. Nagasaki).

https://doi.org/10.1016/j.net.2019.04.017

miles from the Fukushima Daiichi Nuclear Power Plant [10]. The estimated total cost of this disaster is 500 billion U.S. dollars [11], which includes the costs for cleanup and damaged units decommissioning and compensation to the affected people.

NPP have typically been designed and constructed employing deterministic safety approaches, as described by IAEA safety standards (No. SSG-2) [12] and Dawson [13]. Such approaches assume that all the required functions can be achieved during normal and abnormal operation conditions. Although there is a high level of confidence in NPP components when designed using such approaches [14], there is still a probability that a component does not perform as expected under normal operation scenarios, abnormal events, and extreme events, which necessitated adopting probabilistic risk assessment (PRA) approaches. PRA is an analytical technique that integrates the frequency of external/internal events, accident sequences, human reliability analysis, and the probability of components failure in order to evaluate NPP safety, as described in the U.S. Nuclear Regulatory Commission report NUREG/CR-2300 [15].

The U.S. WASH-1400 was the first major PRA framework that investigated many accident sequences in NPP and provided quantitative estimates of the risk associated with these sequences [16]. The WASH-1400 framework uses *static* event and fault tree analysis schemes to simulate the accident sequences following an extreme event. Although such risk assessment techniques have experienced significant improvements, all these improvements essentially followed the WASH-1400 framework developed more than 40 years ago, as illustrated by Mosleh [7], Dawson [13], and Moieni and Spurgin [17]. As such, current risk assessment techniques still have significant fundamental limitations including, for example, the difficulty of developing accident scenarios for NPP risk assessment through event and fault trees, as such prescribed trees might be insufficient in terms of predicting new scenarios. The event and fault tree limitations are partly attributed to the lack of accurate physics representation when NPP systems' dynamic interdependence-induced failures are considered. The limitations are also attributed to the inability to identify the exact timing of the failure-initiating events and the corresponding value of the system variables at such a time [18].

Limitations of current PRA and the occurrence of severe NPP accidents have raised the need to develop adequate methodologies that account for the complexity of hardware/software/operator interactions inside NPP [19]. As such, developing a *dynamic* PRA approach has been identified as key to overcoming the limitations of current PRA. Dynamic PRA is developed in a way that considers the timing and sequencing of events during hardware/software/operator interactions [20], which is essential for NPP risk assessment [21]. Simulation methods of dynamic PRA have been evolving over the past three decades including DYLAM [22], DETAM [23], ADS [24], ADS-IDAC [25], MCDET [26], ADAPT [27], and RAVEN [28]. These platforms, however, need to be integrated with NPP simulators such as RELAP [29] and MELCOR [30] that represent the dynamic behavior of NPP.

1.1. System dynamics simulation approach

In order to improve risk assessment techniques of NPP, there is a need for an integrated platform that simulates the NPP dynamic processes, and thus their responses under abnormal events. In this respect, the current study adopts a system dynamics (SD) simulation approach to assess the dynamic response of different systems in pressurized water reactor (PWR) as a first step in developing an integrated dynamic PRA platform. SD has been adopted in many disciplines, and it is typically used to simulate the dynamic behavior and interdependence within large complex systems, as described by Sonnessa [31], Sterman [32], and Bala et al. [33]. SD was first developed in the 1950s by Jay Forrester as a way to investigate the behavior of complex economic and social systems. Recently, SD has had extensive applications in simulating numerous real-world applications [34]. The concepts of SD are presented in a simplified manner through graphs and basic algebraic formulation rather than complex mathematical/numerical models. For example, Fig. 1 shows a schematic diagram of a PWR SD model, where the feedback loops, stocks, and flows (e.g. the rate of change in stocks) are used to represent the parameters and simulate the PWR's dynamic processes [35]. Feedback loops are key in SD as they control the dynamic interdependence between the different system components, whereas stocks are used to quantify the system parameters at any time. SD is essentially a system of differential equations that are analyzed numerically to simulate the behavior of complex systems [36].

Similar to other disciplines, although not to the same extent, models based on SD have been recently developed for nuclear applications, such as to investigate the nuclear fuel cycle starting from the mining and enrichment processes to repository disposal [37]. In a different study, Jeong and Choi [38] investigated the fuel cycle process in Korea using a SD model and illustrated the importance of using the spent PWR fuel in both the Canada deuterium uranium and sodium-cooled fast reactors in order to reduce the spent fuel inventory. Another recent application of SD was to investigate the effect of generating nuclear power on economic, environmental, political, and social aspects in Singapore [39]. SD was also recently used to investigate the development of nuclear power in China, combining different aspects that have influences on the nuclear power development such as electricity consumption, power generation, and uranium resources [40]. While a SD simulation approach has been used in the above referenced nuclear applications, to date, no study has applied SD to simulate the thermal dynamic processes in a NPP.

The ultimate goal of the current multi-phase study is to develop a dynamic PRA platform to enhance current risk assessment techniques through considering the complex dynamic interdependence between NPP systems/components in one platform. As a first step in this endeavor, the objective of this first phase of the study is to simulate the nonlinear behavior of the thermal dynamic processes in a PWR using SD simulation approach, including the physical responses of multiple interdependent parameters/systems inside a NPP that may lead to system failure, and thus pose a systemic risk. In this respect, three SD models are developed to simulate the nonlinear behavior of the thermal dynamic processes for the reactor core, secondary coolant system and complete PWR based on the PWR behavior described in Thakkar [41], Kerlin et al. [42], Ali [43], Arda et al. [44], Arda [45], and Puchalski et al. [46]. The developed PWR models can later be further integrated with other system models to map the event consequence propagation throughout different NPP systems, thus overcoming the limitations of current static fault and tree event tree analysis schemes in predicting dynamic interdependence-induced systemic risks. A concise background on thermal dynamic processes inside the reactor core and the secondary coolant system (SCS) is provided next. Afterwards, the developed reactor core, SCS, and complete reactor simulation models are validated using the results from published data [45]. Finally, the responses of the developed SD models are evaluated under several different perturbations in primary coolant flow and temperature, external reactivity, and steam valve opening events.

2. System dynamics model development of PWR

The primary function of a PWR is to convert the heat energy

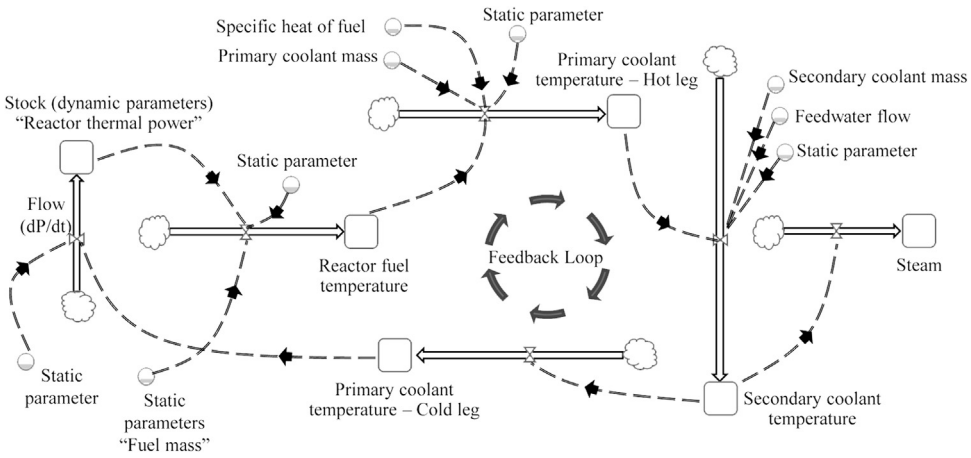

Fig. 1. Schematic diagram of a PWR system dynamics model.

produced by uranium fission to electric power. In the PWR, a reactor pressure vessel (RPV) holds the enriched uranium fuel required for the fission reactions. These reactions take place inside the RPV, generating heat energy and radioactive materials. Next, a high-pressure liquid (water) is circulated in a primary coolant system to cool the reactor core. This results in hot water that leaves the RPV through hot legs to the metal U-tube inside a steam generator. Finally, the steam generator transfers the heat to light-water to produce steam that in turn drives the turbine to generate electricity. A schematic diagram of the PWR generating unit, including the reactor pressure vessel, steam generator, turbine, hot and cold legs, is shown in Fig. 2.

In the current study, SD is used to simulate the thermodynamic process (i.e. the energy production, storage, transfer and conversion) in the PWR, including the reactor core, the plenums, the hot and cold legs, and the steam generator. Three models are established to predict the nonlinear behavior of a complete PWR and validated using the work of Arda [45]. The three models are intended to simulate: 1) the thermodynamic process in the reactor core; 2) the thermodynamic process in the SCS; and 3) the interdependence between the reactor core and the SCS. The reactor core and SCS parameters are based on those of the Palo Verde Nuclear Generating Station [45]. Tables 1 and 2 summarize the reactor core and SCS parameters, respectively. In addition, the delayed neutron fractions β_i and the delayed neutron precursor decay constants λ_i for the six delayed-neutron groups are based on Puchalski et al. [46]. The thermodynamic process is represented in SD models by first-order differential equations. These equations control the interdependency among the different PWR dynamic parameters (e.g. reactor thermal power, reactor fuel and primary coolant temperatures, reactivity of reactor core, metal tube and secondary coolant temperatures, and steam pressure in steam generator) in terms of static parameters such as the heat transfer coefficients, coolant flow, and fuel and coolant masses.

2.1. Model I: Thermal process in the reactor core system

The heat transfer process inside the reactor core is simulated as a function of the reactor core thermal power. This thermal power is represented by point kinetics equations since the reactor power is controlled by reactivity feedbacks due to deviations in fuel, primary coolant temperatures, and external reactivity induced by control rods. Reactivity is assumed to be zero in the reactor steady state operation phase. During the reactor power maneuvering, the reactivity feedback mechanism is controlled by equation (1).

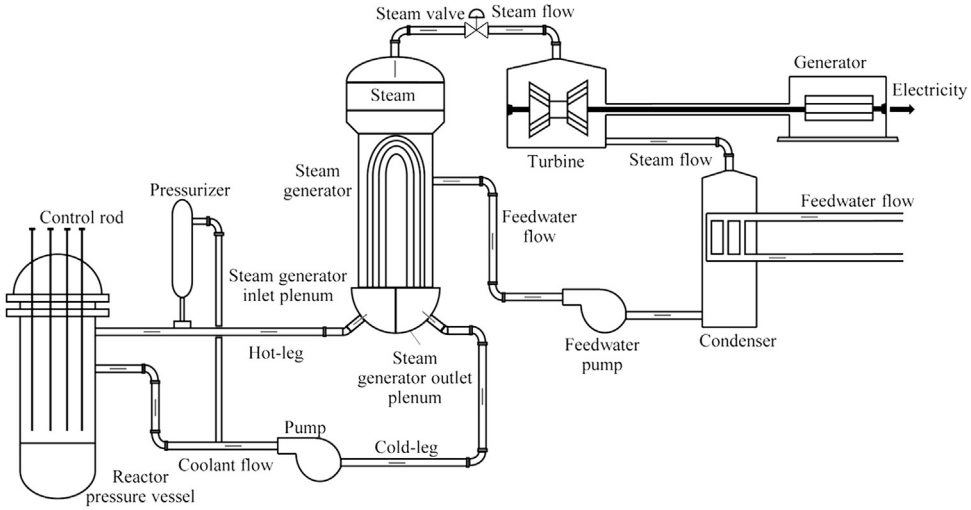

Fig. 2. Schematic diagram of a pressurized water reactor.

Table 1
Parameters for the reactor core system.

P_o	MWth	3800	α_c	1/°F	$-1.0*10^{-4}$	U_{fc}	Btu/hr.ft.°F	325.588
f	–	0.975	α_f	1/°F	$-1.20*10^{-5}$	A_{fc}	ft^2	68600
β	–	0.0065	w_c	lb/hr	$164*10^6$	m_f	lb	$257.1*10^3$
β_1	–	0.000215	λ_1	1/s	0.0124	c_f	Btu/lb.°F	0.1056
β_2	–	0.001424	λ_2	1/s	0.0305	m_c	lb	30721
β_3	–	0.001274	λ_3	1/s	0.1110	c_c	Btu/lb.°F	1.448
β_4	–	0.002568	λ_4	1/s	0.3010	Λ	s	$30*10^{-6}$
β_5	–	0.000748	λ_5	1/s	1.1400			
β_6	–	0.000273	λ_6	1/s	3.0100			

$$\rho(t) = \delta\rho_{ext} + \alpha_F \delta T_F + \frac{\alpha_C}{2}\delta T_{C1} + \frac{\alpha_C}{2}\delta T_{C2} \tag{1}$$

The linearized point kinetics in Eqs. (2) and (3) control the reactor core thermal power with the influence of delayed neutron precursors [47].

$$\frac{d\delta P}{dt} = \frac{-\beta}{\Lambda}\delta P + \sum_{i=1}^{6}\lambda_i \delta C_i(t) + \frac{P_0}{\Lambda}\delta\rho_{ext} + \frac{\alpha_F P_0}{\Lambda}\delta T_F + \frac{\alpha_C P_0}{2\Lambda}\delta T_{C1} + \frac{\alpha_C P_0}{2\Lambda}\delta T_{C2} \tag{2}$$

$$\frac{d\delta C_i(t)}{dt} = \frac{\beta_i}{\Lambda}\delta P - \lambda_i \delta C_i\ ,\ i = 1, \ldots, 6 \tag{3}$$

The current study utilizes Mann's model [48] to represent the deviation in the primary coolant and fuel temperatures. As shown in Fig. 3, this model includes one node for the uranium fuel temperature and two nodes for the primary coolant temperature. In the reactor steady state operation phase, the reactor thermal power is constant and there is no deviation in the reactor fuel and coolant temperatures. As such, fluctuation in the reactor thermal power is achieved by changing the reactor core parameters such as the inlet coolant temperature, external reactivity, and primary coolant flow. Afterwards, the feedback mechanism causes a deviation in the overall PWR response. The reactor core parameters used in the current study are provided in Table 1, as mentioned earlier. Equation (4) represents the deviation in the reactor fuel temperature, while Eqs. (5) and (6) control the deviation in the coolant temperature nodes from the steady state.

$$\frac{d\delta T_F}{dt} = \frac{f}{m_f c_f}\delta P - \frac{U_{FC}{}^* A_{FC}}{m_f c_f}(\delta T_F - \delta T_{C1}) \tag{4}$$

$$\frac{d\delta T_{c1}}{dt} = \frac{1-f}{m_c c_c}\delta P - \frac{U_{FC}{}^* A_{FC}}{m_c c_c}(\delta T_F - \delta T_{C1}) - \frac{2w_c}{m_c}(\delta T_{c1} - \delta T_{LP}) \tag{5}$$

$$\frac{d\delta T_{c2}}{dt} = \frac{1-f}{m_c c_c}\delta P - \frac{U_{FC}{}^* A_{FC}}{m_c c_c}(\delta T_F - \delta T_{C1}) - \frac{2w_c}{m_c}(\delta T_{c2} - \delta T_{c1}) \tag{6}$$

The thermal dynamic process of the reactor core is simplified in the current study using the following assumptions [46]: 1) the fuel to coolant heat transfer coefficient is constant; 2) the coolant flow is one dimensional; and 3) the coolant is a single phase with constant density and specific heat.

The dynamic parameters of the reactor core (e.g., fuel and coolant temperatures, reactor thermal power, and reactivity) are modeled using stocks. The rates of change of these parameters are controlled by the feedback from multiple dynamic parameters and static parameters such as the fuel and coolant masses, heat transfer coefficient, and coolant flow, as shown in Fig. 4.

Table 2
Parameters for the secondary coolant system.

τ_{P1}	s	1.2815	$\delta T_{SAT}/\delta P$	°F/psi	0.1176	m_{sw}	lb	334000
τ_{P2}	s	1.2815	$\delta h_f/\delta P$	Btu/lb.psi	0.1508	m_{ss}	lb	36904
τ_{PM1}	s	1.2233	$\delta h_g/\delta P$	Btu/lb.psi	−0.0385	P_{so}	psi	1070
τ_{PM2}	s	0.5826	$\delta v_g/\delta P$	ft^3/lb.psi	$-4.64*10^{-4}$	c_{pi}	Btu/lb.°F	1.278
τ_{MP1}	s	0.3519	h_g	Btu/lb	1189	w_{so}	lb/hr	$17.18*10^6$
τ_{MP2}	s	0.1676	h_f	Btu/lb	554	c_m	Btu/lb.°F	0.10205
τ_{MS1}	s	0.3519	v_f	ft^3/lb	0.0218	T_{fi}	°F	450
τ_{MS2}	s	0.1676	v_g	ft^3/lb	0.4114	C_L	–	6

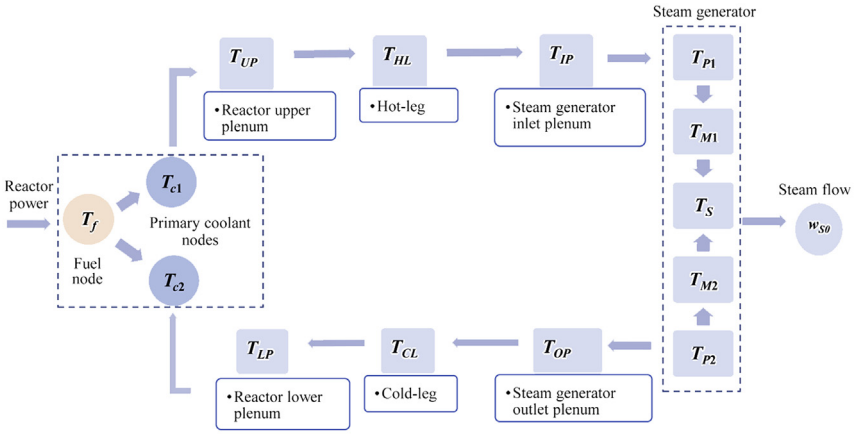

Fig. 3. Schematic diagram of a PWR thermal dynamic process.

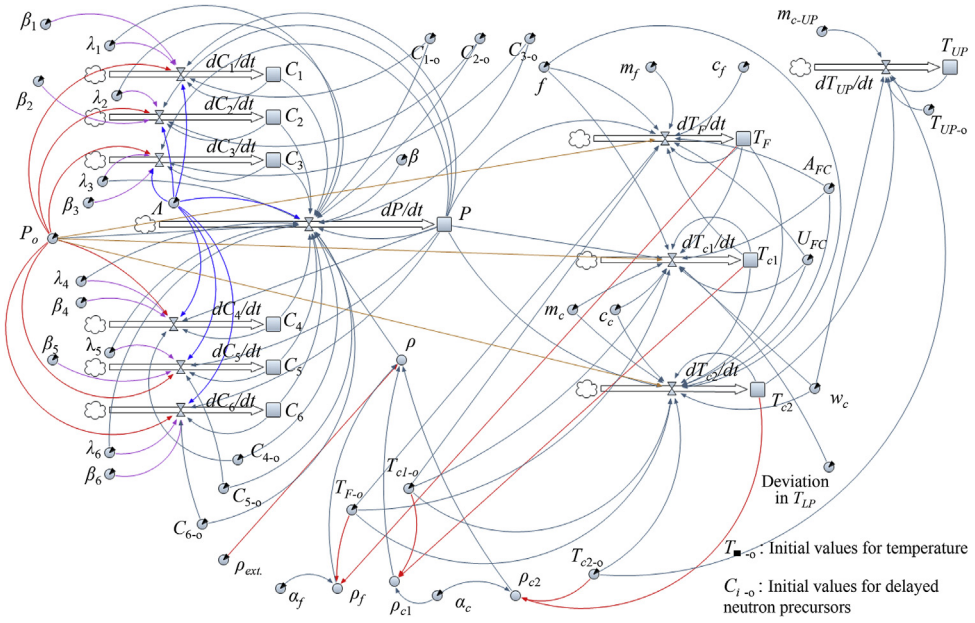

Fig. 4. Model I: system dynamics of the thermal dynamic process in the reactor core.

2.2. Model II: Thermal process in the secondary coolant system

The steam generator contains a number of metal U-tubes for the primary coolant flow process. These tubes are essential components that separate the secondary and primary coolants in order to prevent the transfer of radioactive material to the SCS. The primary function of the steam generator is to convert the heat energy stored in the primary coolant into electric power. This is performed by boiling the water inside the steam generator to produce steam that drives the turbine of an electric generator. Next, this steam is condensed and returned to the steam generator.

The thermodynamic process in the steam generator consists of two heat transfer processes. First, the heat stored in the primary coolant is transferred to the metal tubes. Second, the heat is transferred from the metal U-tubes to the secondary coolant. A simplified simulation for the thermodynamic process in the steam generator is performed by representing the SCS using five lumps, as shown in Fig. 3. The primary coolant and U-tubes are each represented by two lumps to simulate the two branches of U-tubes, while the secondary coolant is simulated by only one lump.

Several aspects of the thermodynamic process in the steam generator are considered [30,32]: 1) the heat transfer coefficients are constant during the reactor fluctuations; 2) the thermal conductivity of the steam generator metal U-tubes is constant; 3) the coolant flow is one-dimensional; 4) the properties of the saturated water and steam are constant over the steam pressure range of 600–1000 psi; 5) the feedwater flow is controlled (i.e. the feedwater flow is equal to the steam flow); and 6) and the steam flow rate is controlled only by the steam generator pressure (i.e. critical flow assumption).

In order to simulate the heat transfer process inside the steam generator using SD, the differential equations of the SCS dynamic parameters (e.g. primary coolant, metal U-tubes, secondary coolant temperatures, and steam pressure) are adopted using the following physical phenomena [45]: 1) heat balance for primary fluid; 2) heat balance for metal tube; 3) secondary fluid (liquid and steam phase) mass balance; 4) steam generator volume balance (i.e. the change of secondary coolant volume plus the change in the steam volume is zero); and 5) secondary fluid (liquid and steam phase) energy balance. Algebraic substitutions are also performed to yield the following differential equations. After linearization, deviations in primary coolant and metal U-tube lump temperatures are expressed by Eqs. (7)–(10), respectively. Finally, Eqs. (11) and (12) represent the deviation in the steam pressure inside the steam generator. The steam generator parameters used in the current study are provided in Table 2. The steam valve coefficient (C_L) in the SD model is calibrated to predict the thermal dynamic behavior of the SCS similar to that of Arda's model because this coefficient is not reported in Arda [45].

$$\frac{d\delta T_{P1}}{dt} = \frac{1}{\tau_{P1}}\delta T_{PI} - \left(\frac{1}{\tau_{PM1}} + \frac{1}{\tau_{P1}}\right)\delta T_{P1} + \frac{1}{\tau_{PM1}}\delta T_{M1} \tag{7}$$

$$\frac{d\delta T_{P2}}{dt} = \frac{1}{\tau_{P2}}\delta T_{P1} - \left(\frac{1}{\tau_{PM2}} + \frac{1}{\tau_{P2}}\right)\delta T_{P2} + \frac{1}{\tau_{PM2}}\delta T_{M2} \tag{8}$$

$$\frac{d\delta T_{M1}}{dt} = \frac{1}{\tau_{MP1}}\delta T_{P1} - \left(\frac{1}{\tau_{MS1}} + \frac{1}{\tau_{MP1}}\right)\delta T_{M1} + \frac{1}{\tau_{MS1}}\left(\frac{\partial T_{SAT}}{\partial P}\right)\delta P_S \tag{9}$$

$$\frac{d\delta T_{M2}}{dt} = \frac{1}{\tau_{MP2}}\delta T_{P2} - \left(\frac{1}{\tau_{MS2}} + \frac{1}{\tau_{MP2}}\right)\delta T_{M2} + \frac{1}{\tau_{MS2}}\left(\frac{\partial T_{SAT}}{\partial P}\right)\delta P_S \tag{10}$$

$$\frac{d\delta P_S}{dt} = \frac{1}{K}\left[U_{ms}S_{ms1}\delta T_{M1} + U_{ms}S_{ms2}\delta T_{M2} - \left[(U_{ms}S_{ms1} + U_{ms}S_{ms2}) \times \left(\frac{\partial T_{SAT}}{\partial P}\right) + w_{so}\frac{\partial T_{SAT}}{\partial P} + C_L\left(h_g - c_{pi}T_{fi}\right)\right]\delta P_S\right] + w_{so}c_{pi}\delta T_{fi} - P_{so}\left(h_g - c_{pi}T_{fi}\right)\delta C_L \tag{11}$$

$$K = \left(m_{sw}\frac{\partial h_f}{\partial P} + m_{ss}\frac{\partial h_g}{\partial P} - m_{ss}\frac{h_{fg}}{v_{fg}}\frac{\partial v_g}{\partial P}\right) \tag{12}$$

Stocks are used to represent the primary coolant, metal U-tube

lump temperatures, and steam pressure. Equations (7)–(12) provide the rates of change of these parameters. All other parameters (e.g. coolant residence time, mass of coolant, coolant flow, and mass of metal lump) are considered as static parameters for simplicity of the model. As can be seen in Fig. 5, the SD model of the SCS shows feedback loops between the system dynamic parameters (i.e. stocks) and the static parameters.

2.3. Model III: Thermal process in The pressurized water reactor

The thermal dynamic process for the reactor core upper (outlet) and lower (inlet) plenums, steam generator outlet and inlet plenums, and the hot and cold legs are combined with the reactor core and SCS models to present a better representation for the whole PWR, as shown in Fig. 6. The primary coolant residence time values inside the plenums, cold and hot legs are provided in Table 3. Following the thermodynamics procedure, the linearized differential equations (Eqs. (13)–(18)) are extracted. More specifically, Eqs. (13) and (14) define the coolant temperature deviation in the upper reactor core and lower plenums, while Eqs. (15) and (16) represent the coolant temperature deviation in the inlet and outlet steam generator. Finally, Eqs. (17) and (18) provide the coolant temperature deviation in the hot and cold legs.

$$\frac{d\delta T_{UP}}{dt} = \frac{1}{\tau_{UP}}(\delta T_{c2} - \delta T_{UP}) \tag{13}$$

$$\frac{d\delta T_{LP}}{dt} = \frac{1}{\tau_{LP}}(\delta T_{CL} - \delta T_{LP}) \tag{14}$$

$$\frac{d\delta T_{IP}}{dt} = \frac{1}{\tau_{IP}}(\delta T_{HL} - \delta T_{IP}) \tag{15}$$

$$\frac{d\delta T_{OP}}{dt} = \frac{1}{\tau_{OP}}(\delta T_{P2} - \delta T_{OP}). \tag{16}$$

$$\frac{d\delta T_{HL}}{dt} = \frac{1}{\tau_{HL}}(\delta T_{UP} - \delta T_{HL}). \tag{17}$$

$$\frac{d\delta T_{CL}}{dt} = \frac{1}{\tau_{CL}}(\delta T_{OP} - \delta T_{CL}) \tag{18}$$

3. System dynamics model validation of PWR

3.1. Model I: The reactor core system

The thermal dynamic process in the reactor core is validated under an increase in the external reactivity (ρ_{ext}) by 7.3×10^{-5} at 10 s, to facilitate a direct comparison with available data [45]. This action is followed by an increase in the neutron flux that subsequently causes an immediate increase in the reactor thermal power. After reactor stability, the reactor core thermal power increases to 24.8 and 27.9 MWth in the SD model and Arda's model, respectively, as shown in Fig. 7-a. Increasing the thermal power of the reactor core is accompanied by an increase in the temperatures of the fuel and coolant nodes, as shown in Fig. 7-b. This initiates negative reactivity feedback that drives the total reactivity to decrease. As can be seen in Fig. 7-a, although the SD model shows a considerable difference in thermal power relative to Arda's model immediately after the increase in external reactivity at 10 s, the reactor power after stabilization is simulated accurately by the SD model with a deviation of only 11%. As shown in Fig. 7-b, the reactor fuel and coolant temperature values estimated by the SD model are lower than those calculated from Arda's model by 11%.

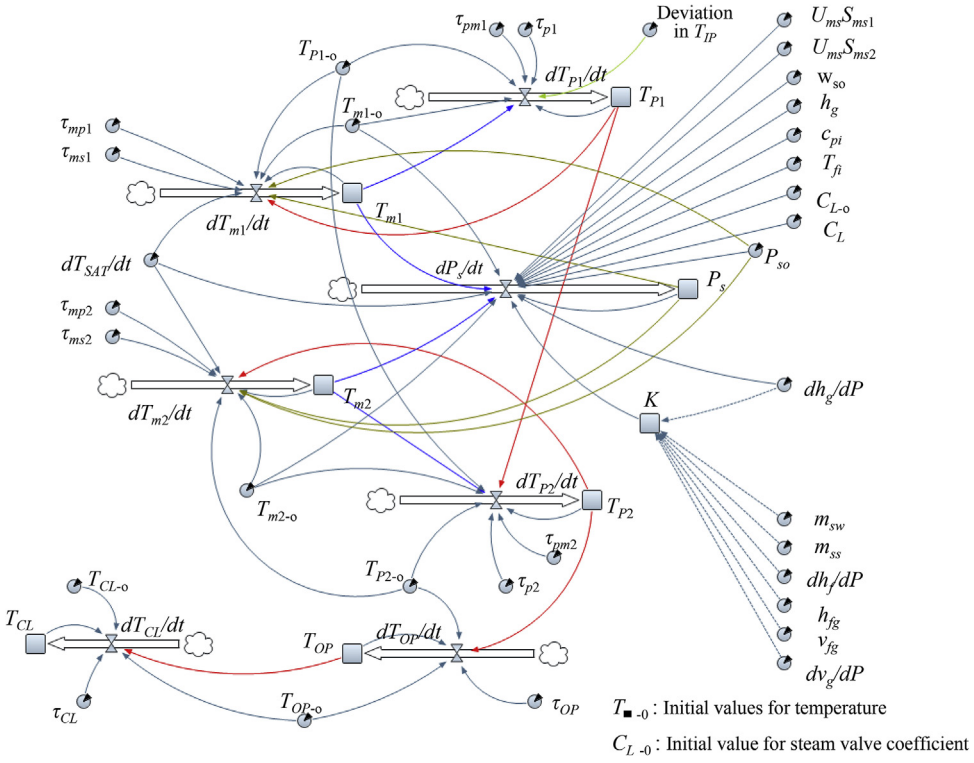

Fig. 5. Model II: system dynamics of the thermal dynamic process in the secondary coolant system.

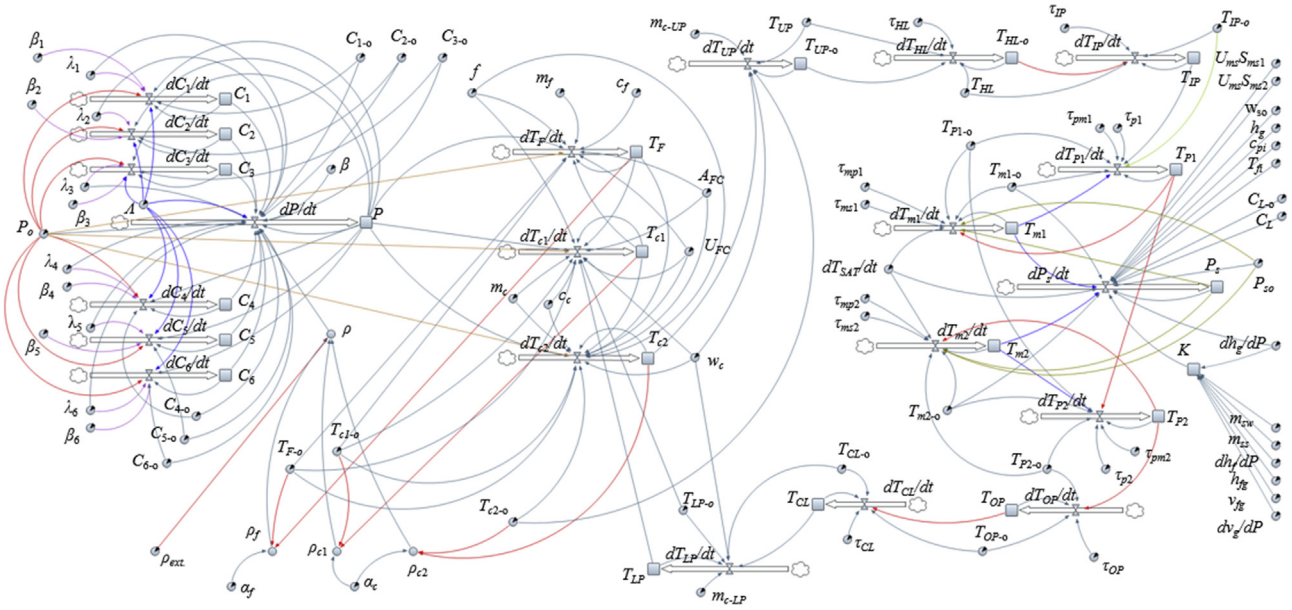

Fig. 6. Model III. system dynamics of the complete thermal dynamic process in PWR.

Table 3
Parameters for plenums, hot and cold legs.

τ_{UP}	s	2.517	τ_{OP}	s	0.726
τ_{HL}	s	0.234	τ_{CL}	s	1.310
τ_{IP}	s	0.659	τ_{LP}	s	2.145

3.2. Model II: The secondary coolant system

The thermal dynamic process in the SCS is validated under an increase in the inlet coolant temperature (T_{IP}) by 10 °F at 5 s without changing the steam valve coefficient (C_L). This is followed by an increase in the temperature of the primary coolant lumps (T_{P1}, T_{P2}). Additional heat is transferred from the primary coolant to the metal U-tubes. As a result, the temperature of these tubes increases and additional heat energy is transferred to the secondary coolant, which in turn generates additional steam. Fig. 8-a shows similar increases in the coolant (T_{P1}) and metal U-tube (T_{m1}) temperatures after an increase in the inlet coolant temperature in both the SD model and Arda's model. Subsequently, as can be seen in Fig. 8-b, the steam pressure in the steam generator increases because the steam valve opening is maintained constant. The dynamic parameters of the SCS (i.e. primary coolant, metal tube temperatures, and steam pressure) in the SD model and Arda's model show a similar nonlinear dynamic response after an increase in the inlet coolant temperature. As can be seen in Fig. 8-b, the steam pressure is increased by 51.1 and 52.4 psi in the SD model and Arda's model, respectively, a minor deviation of only 2.5%.

3.3. Model III: The pressurized water reactor

The complete thermodynamic process in the PWR is validated under an increase in the external reactivity. This investigates the dynamic response of different parameters in the SCS to small perturbations inside the reactor core. A positive reactivity of 7.3×10^{-5} is applied at 10 s without changing the steam valve coefficient. As shown in Fig. 9-a, the reactor fuel temperature increases following the increase of the external reactivity. This causes more heat energy to be transferred from the primary coolant system to the SCS. As a result, additional steam is produced that causes an increase in the steam pressure, as shown in Fig. 9-b. It should be noted that the reactor core inlet coolant temperature (T_{LP}) increases after a complete primary coolant cycle, as shown in Fig. 9-a, which in turn causes high negative reactivity feedback. As such, the fuel temperature decreases after reaching the maximum value in both the SD model and Arda's model, with a maximum difference between

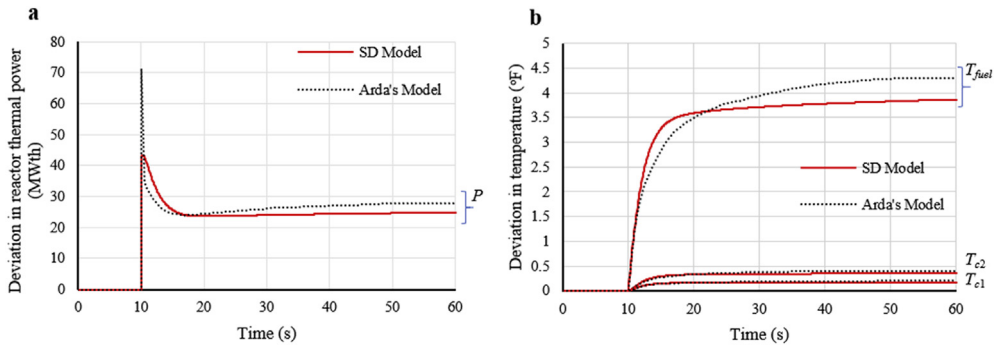

Fig. 7. a. Reactor thermal power response due to adding positive reactivity (Model I). b. Fuel and coolant nodes temperature response due to adding positive reactivity (Model I).

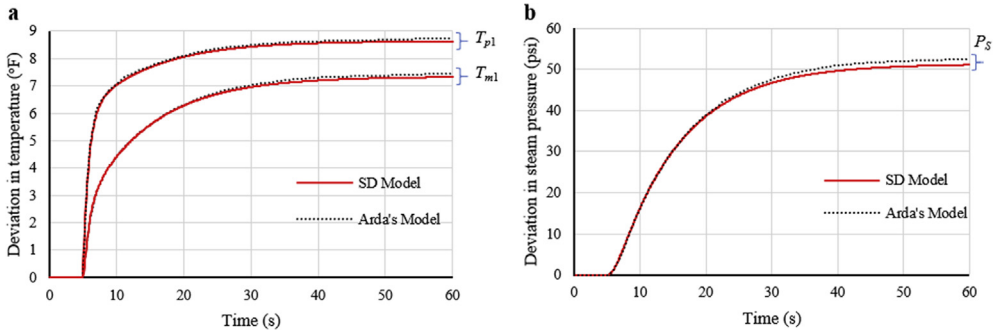

Fig. 8. a. Primary coolant (T_{p1}) and metal U-tube (T_{m1}) temperature response due to an increase in inlet coolant (T_{IP}) temperature (Model II). b. Steam pressure response due to an increase in inlet coolant (T_{IP}) temperature (Model II).

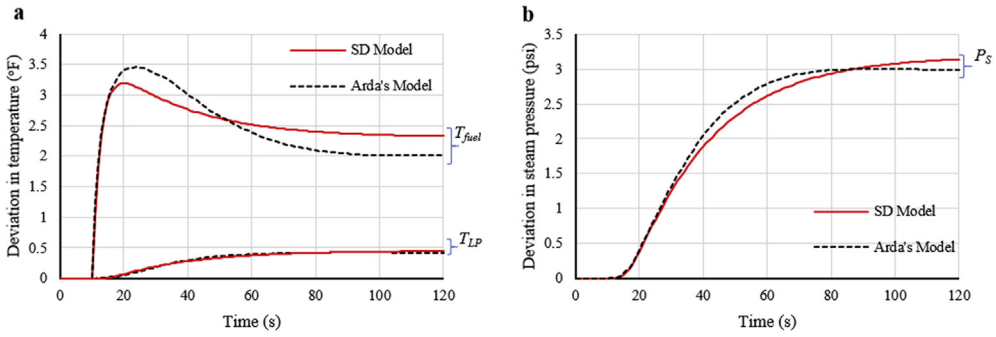

Fig. 9. a. Fuel and inlet coolant (T_{LP}) temperature response due to adding positive reactivity (Model III). b. Steam pressure response due to adding positive reactivity (Model III).

the two models of 15%. As can be seen in Fig. 9-b, the steam pressure in the SCS after a positive change in the external reactivity shows similar responses (within 5%) in the SD model and Arda's model.

4. Perturbation event effects on thermal dynamic process in the PWR

Following the SD model validation, the thermal dynamic processes in the reactor core, SCS, and complete PWR are tested separately under different perturbation events to verify the interaction among feedback mechanisms. These events include either single or multiple actions at a specific time or actions that fluctuate with time.

4.1. Model I: The reactor core system

The response of reactor thermal power, coolant, and fuel temperatures are investigated due to a change in: 1) the external reactivity (ρ_{ext}) induced by the control rod; 2) the inlet core coolant temperature (T_{LP}); and 3) the primary coolant mass flow (w_c).

In the first event, the external reactivity is increased by 7.3×10^{-5} at 10 s. Simultaneously, three different scenarios are carried out to investigate the influence of the primary coolant mass flow on the thermal dynamic behavior of the reactor core. More specifically, the primary coolant flow (wc) is maintained constant in the first scenario, while this flow is increased and reduced by 20% in the second and third scenarios, respectively. As shown in Fig. 10-a, the reactor thermal power is immediately increased after adding a positive reactivity, a behavior that is observed in all scenarios. As the thermal power increases, the reactor fuel and primary coolant temperatures increase, as shown in Fig. 10-b, causing negative reactivity feedback. Also, Fig. 10-b shows that the low value of the coolant mass flow in the third scenario (0.8 wc) leads to an increase in the coolant temperature relative to the first and second scenarios. In particular, the third scenario shows higher negative reactivity feedback as expected, which leads to a reduction in the reactor thermal power by 8.6% compared to the first scenario, respectively. Increasing the primary coolant flow has the opposite effect of reducing the negative reactivity feedback, leading to a relative increase in the reactor thermal power.

The second event investigates the dynamic parameters of the reactor when the control rods are inserted (i.e. a 7.3×10^{-5} decrease of reactivity). Fig. 11-a shows an immediate drop in the thermal power of the reactor core, which then stabilizes to 15.7 MWth. This behavior is attributed to the control rods that capture neutrons, and simultaneously, the fuel and coolant nodes temperatures are decreased. As can be seen in Fig. 11-b, the reactor fuel and coolant nodes (T_{C2}, T_{C1}) temperatures decrease by 2.44 °F, 0.22 °F, and 0.1 °F, respectively.

In the third event, the temperature of the inlet coolant (T_{LP}) is increased by 5 °F at 10 s. This is followed by high negative reactivity feedback that induces a significant drop in the reactor thermal power. As can be noted from Fig. 12-a, the reactor thermal power stabilizes because of the negative reactivity feedback with a reduction in its initial value by 120 MWth. In addition, Fig. 12-b shows a reduction in the fuel temperature by 13.7 °F in response to the increase in the inlet coolant temperature, because of the thermal power reduction.

4.2. Model II: The secondary coolant system

Fluctuations in steam pressure, primary coolant, and metal U-tube lump temperatures are investigated during several events.

In the first event, the steam valve coefficient (C_L) is decreased by 5% at 5 s. As can be seen in Fig. 13-a, this event is followed by an

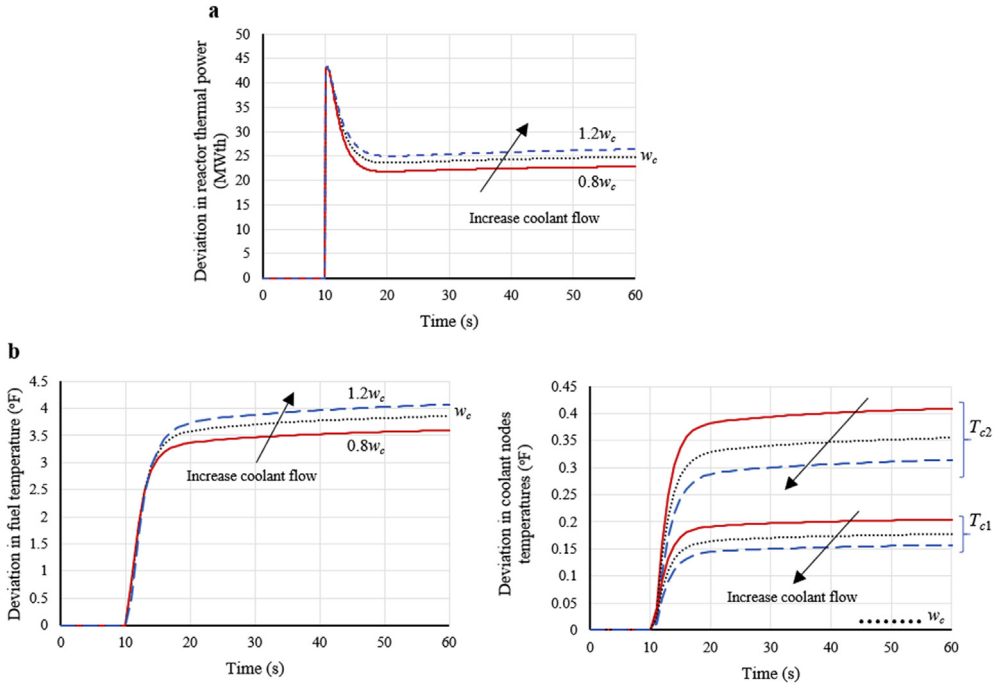

Fig. 10. a. Reactor thermal power response due to adding positive reactivity for different primary coolant flow (*wc*) values (Model I – 1st Event). b. Fuel and coolant nodes temperature response due to adding positive reactivity for different primary coolant flow (*wc*) values (Model I – 1st Event).

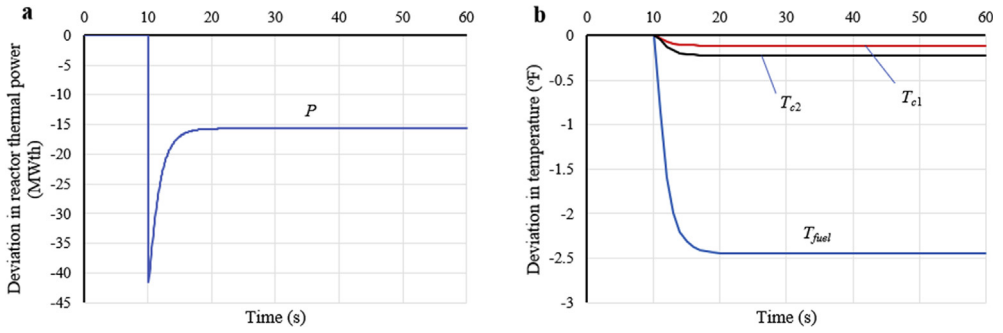

Fig. 11. a. Reactor thermal power response due to adding negative reactivity (Model I – 2nd Event). b. Fuel and coolant nodes temperature response due to adding negative reactivity (Model I – 2nd Event).

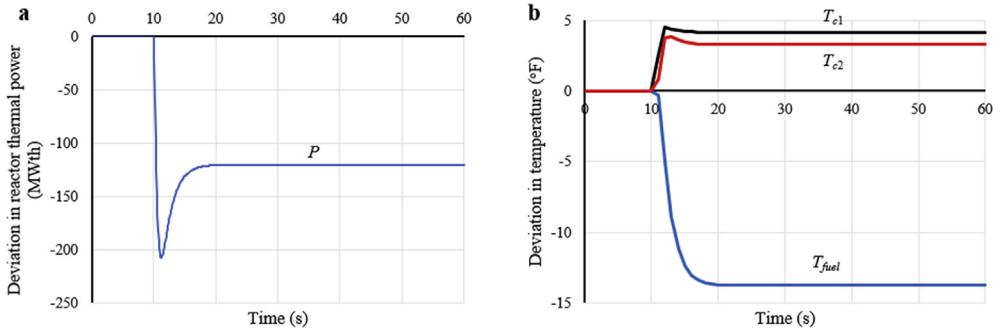

Fig. 12. a. Reactor thermal power response due to an increase in the inlet coolant (T_{LP}) temperature by 5 °F (Model I – 3rd Event). b. Fuel and coolant nodes temperature response due to an increase in the inlet coolant (T_{LP}) temperature by 5 °F (Model I – 3rd Event).

immediate increase in the steam pressure inside the steam generator. Then, a small amount of heat is transferred from the primary coolant system to the SCS followed by increases in the coolant and metal tube lump temperatures, as shown in Fig. 13-b.

In the second event, the temperature of the steam generator inlet coolant (T_{IP}) is increased by 10 °F at 5 s. Simultaneously, three different scenarios are applied to investigate the influence of the steam valve opening position on the thermodynamic behavior of

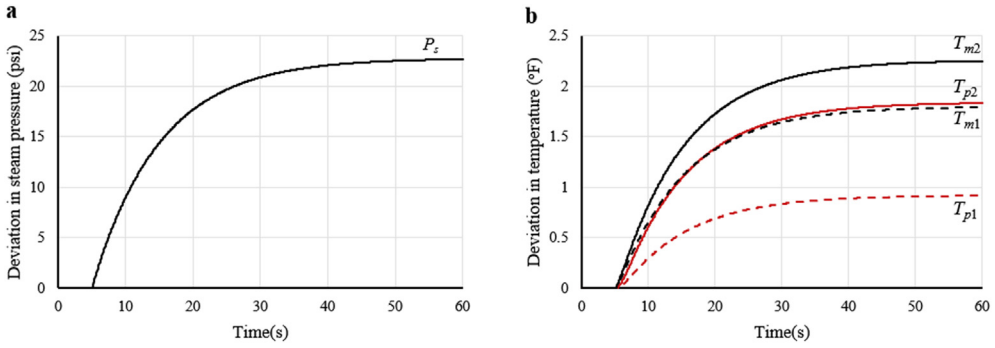

Fig. 13. a. Steam pressure response due to a decrease in steam valve coefficient by 5% (Model II – 1st Event). b. Primary coolant and metal tube lump temperature response due to a decrease in steam valve coefficient by 5% (Model II – 1st Event).

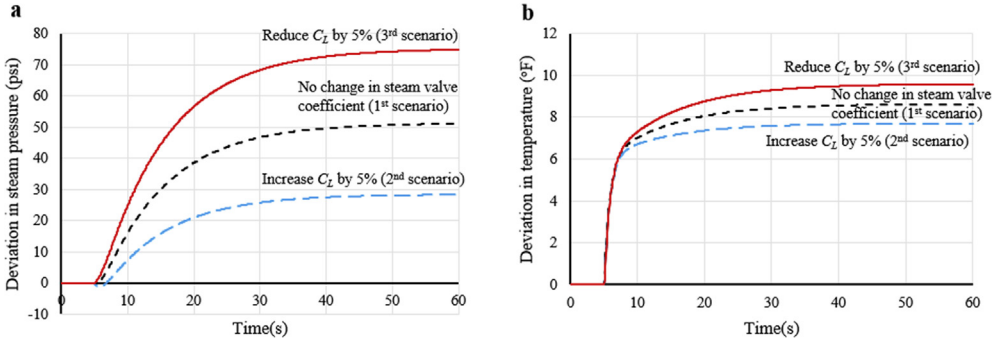

Fig. 14. a. Steam pressure response due to an increase in inlet temperature (T_{IP}) by 10 °F with different steam valve (C_L) coefficient (Model II – 2nd Event). b. Primary coolant lump (T_{p1}) temperature response due to an increase in inlet temperature (T_{IP}) by 10 °F with different steam valve (C_L) coefficient (Model II – 2nd Event).

the SCS. In the first scenario, the steam valve coefficient is maintained constant, while the same coefficient is increased and decreased by 5% in the second and third scenarios, respectively. As shown in Fig. 14-a, an immediate slight reduction in steam pressure is observed in the case of the steam valve opening (i.e. second scenario), followed quickly by a much larger increase in steam pressure as more heat is transferred from the primary to the secondary system following the increase in the inlet coolant temperature. As can be seen also in Fig. 14-b, the primary coolant lump 1 (T_{P1}) temperature is lower for the second scenario compared to other scenarios. This is because more steam is required due to the opening of the steam valve, leading to more heat energy being transferred from the primary coolant system, and therefore, a smaller increase in primary coolant temperature. In summary, the increase in the steam valve coefficient reduces both the steam pressure and primary coolant temperature compared to the first and third scenarios.

4.3. Model III: The pressurized water reactor

Following the evaluation of the reactor core and the SCS to different perturbation events, a SD model of the complete thermodynamic process is essential to predict the response of the steam generator when perturbation events occur inside the reactor core and vice versa. This SD model is developed by combining the aforementioned reactor core and SCS thermal dynamic models, as described earlier. In this subsection, the thermal dynamic process of a complete PWR is investigated under three different perturbation events.

First, a small perturbation is applied by increasing the steam valve coefficient by 5% at 5 s. Therefore, additional steam is expected to be produced in order to balance the SCS thermal dynamic process. This event is followed by a reduction in the steam pressure (P_S) and temperature (T_{steam}) values by 29.1 psi and 3.4 °F, as shown in Fig. 15-a and 15-b, respectively. More heat is transferred from the primary coolant in the U-tube to the secondary system in order to accommodate the steam generation, and subsequently, the primary coolant lump temperatures (T_{P1}, T_{P2}) are reduced. This behavior is followed by a reduction in the reactor core inlet primary coolant temperature (T_{LP}). Also, Fig. 15-b shows that the reactor core primary coolant temperatures (T_{c1}, T_{c2}) are reduced by 2.1 °F and 1.4 °F, respectively. The reduction in coolant temperature causes positive reactivity feedback that leads to an increase in the reactor thermal power by 97 MWth, as shown in Fig. 15-a. Fig. 15-b also shows that the reactor fuel temperature is increased by 12.3 °F because of this increase in the reactor thermal power.

The second event investigates different steam valve opening positions after a positive reactivity of 7.3×10^{-5} is added. The first scenario is applied without changing the steam valve coefficient, while the steam valve coefficient is increased and decreased by 5% in the second and third scenarios, respectively. All scenarios show an immediate increase in the reactor thermal power (Fig. 16-b), and subsequently, the fuel temperature (Fig. 16-c) increases after the external reactivity is added. However, in the third scenario, the reduction in the steam valve coefficient results in negative reactivity feedback, primarily because of an increase in the reactor core inlet coolant temperature. As can be seen in Fig. 16-a, a reduction in the steam valve coefficient (third scenario) by 5% causes an increase in the reactor inlet coolant temperature (T_{LP}) by 4.0 °F. Because of the negative reactivity feedback in this scenario, the thermal power is reduced by 81.6 MWth relative to the first scenario. On the other hand, Fig. 16-b shows an increase in the reactor thermal power by 95 MWth relative to the first scenario after an increase in the steam valve coefficient. In this second scenario, the reactor core thermal

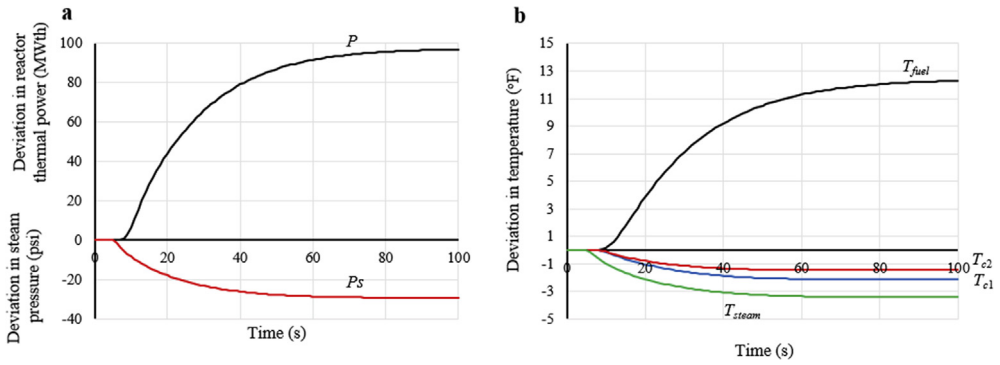

Fig. 15. a. Reactor thermal power and steam pressure response due to an increase in steam valve coefficient by 5% (Model III – 1st Event). b. Fuel, coolant nodes, steam temperature response due to an increase in steam valve coefficient by 5% (Model III – 1st Event).

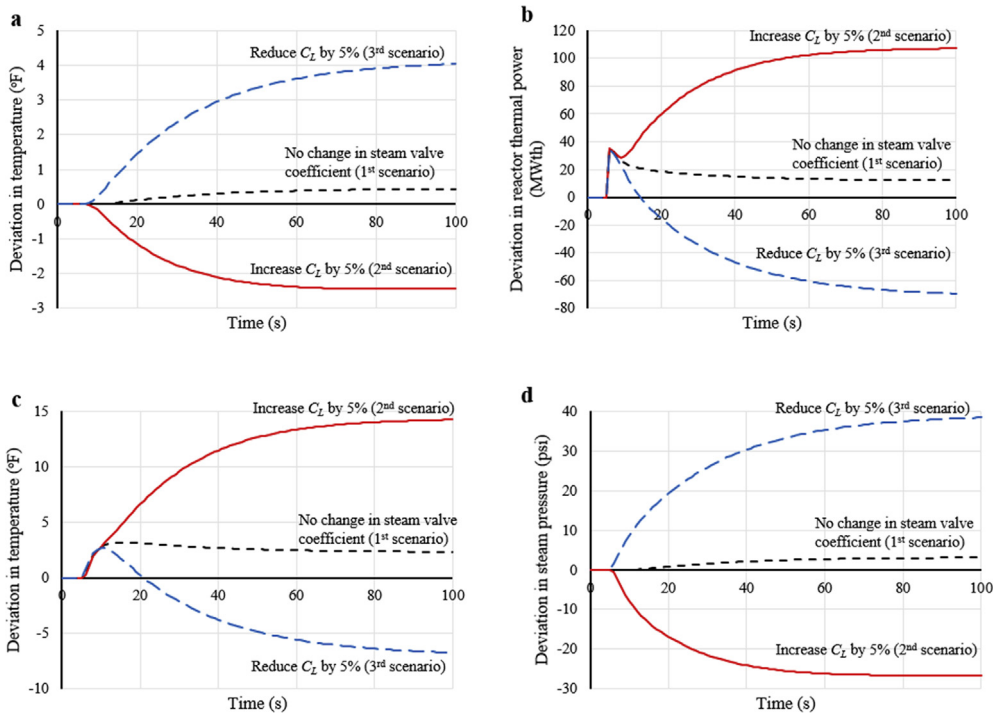

Fig. 16. a. Inlet coolant (T_{LP}) temperature response due to adding positive reactivity with different steam valve coefficient (C_L) (Model III – 2nd Event). b. Reactor thermal power response due to adding positive reactivity with different steam valve coefficient (C_L) (Model III – 2nd Event). c. Fuel temperature response due to an increase in reactivity with different steam valve coefficient (C_L) (Model III – 2nd Event). d. Steam pressure response due to an increase in reactivity with different steam valve coefficient (C_L) (Model III – 2nd Event).

power reaches a peak value, then drops as a result of the decay of fission fragments, and finally, the reactor power starts increasing again due to the feedback of increasing the steam valve coefficient. It is clear from Fig. 16-c that the reactor fuel temperature is significantly reduced in the third scenario as a result of the negative reactivity feedback. Fig. 16-b and 16-d show that closing the steam valve by 5% reduces the thermal power of the reactor core by 81.6 MWth and increases the steam pressure by 35.3 psi relative to the first scenario, in which the deviations in the reactor thermal power and steam pressure are 12.2 MWth and 3.1 psi, respectively. On the other hand, increasing the steam valve coefficient leads to a reduction in the steam pressure by 29.6 psi and an increase in the thermal power by 95 MWth relative to the first scenario.

In the third and final event, a positive reactivity of 6.5×10^{-5} is applied for a 30 s interval through a constant steam valve coefficient, followed by a 30 s interval of zero reactivity, as shown in Fig. 17-a. This external reactivity event is mainly to investigate the nonlinear response of the reactor thermal power to the change in the position of control rods within this time frame (i.e. up to 180 s). Fig. 17-b shows an increase in the fuel, coolant nodes, and steam temperatures after the reactivity is increased. Removal of the external reactivity reduces the total reactivity immediately due to the negative fuel and coolant temperature reactivity feedback. As can be seen in Fig. 17-c, the thermal power fluctuates immediately after changing the external reactivity. The cumulative behavior of the reactor parameters shows an increase in the thermal power, as well as the fuel and coolant temperatures. Fig. 17-d shows also an increase in the steam pressure since the increase in the coolant temperature transfers additional heat energy from the primary coolant system to the secondary system.

5. Conclusions

A nuclear power plant (NPP) contains multiple systems that

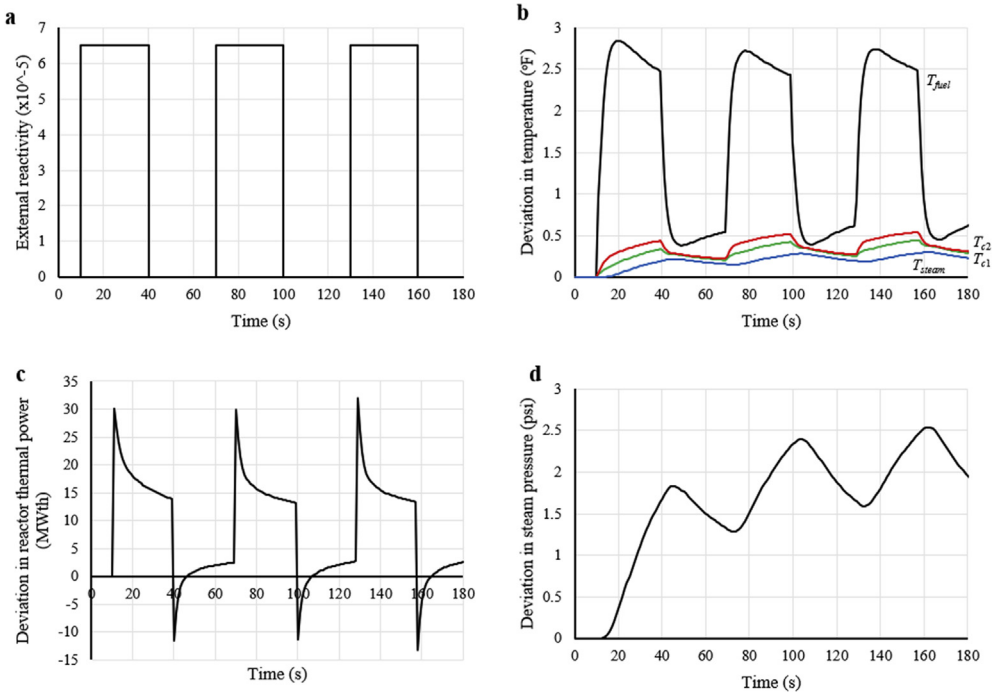

Fig. 17. a. Fluctuation in external reactivity every 30 s (Model III – 3rd Event). b. Fuel, coolant, and steam temperature response due to adding positive reactivity every 30 s (Model III – 3rd Event). c. Reactor thermal power response due to adding positive reactivity every 30 s (Model III – 3rd Event). d. Steam pressure response due to adding positive reactivity every 30 s (Model III – 3rd Event).

interact through several feedback mechanisms to generate electricity. The complex dynamic interdependence among these systems, the consequence and severity of interacting hazards, and the drawbacks of current static risk assessment techniques in terms of addressing dynamic interdependence-induced systemic risks have raised major concerns about NPP safety, especially after the Fukushima Daiichi disaster. To address these concerns, a system dynamics (SD) approach was used to simulate the thermal dynamic processes within different systems inside a pressurized water reactor (PWR), as the first step to overcome the limitation of current risk assessment techniques of NPPs. Three SD models of the reactor core, secondary coolant system (SCS), and complete PWR were validated against the results of a previously published work. Subsequently, these models were evaluated under different perturbation events pertaining to the external reactivity, primary coolant flow, and the steam valve coefficient. The results obtained from the complete PWR model, combining the reactor core and SCS, were used to investigate the impact of interconnectivity and nonlinear feedback mechanism between different systems inside the PWR.

The results of the current study demonstrate the capability of the SD approach to simulate the physical processes between major interdependent systems in NPPs under different perturbation events. These physical processes are represented by the reactor thermal power, fuel and coolant temperatures and steam pressure. Moreover, the developed SD simulation approach provides significant advantages from both the time and data storage perspectives, since the analysis of the developed SD models was very fast (e.g. the time needed for the longest perturbation event analysis is less than 60 s) with a very modest size of output data (e.g. the generated data for all perturbation events for both validation and evaluation analysis conducted in the current study was less than 500 KB). In this respect, SD is expected to facilitate the development of systemic risk assessment techniques supported by feedback loops that facilitates accurate simulation of several complex dynamic accident scenarios. Thus, the current study presents the first phase in a multi-phase research program aimed at developing dynamic probabilistic systemic risk assessment platform that takes into account the interaction and interdependence of different NPP systems with an ultimate goal of enhancing the overall NPP safety and resilience in a multi-hazard environment.

Acknowledgments

The financial support for the study was provided through the Canadian Nuclear Energy Infrastructure Resilience under Systemic Risks (CaNRisk) – Collaborative Research and Training Experience (CREATE) program of the Natural Science and Engineering Research Council (NSERC) of Canada.

Notation

A_{FC}	Effective heat transfer surface area between the reactor fuel and primary coolant
c_c	Specific heat of primary coolant
c_f	Specific heat of the reactor fuel
C_i	Delayed neutron precursors, $i = 1,\ldots\ldots,6$
C_L	Steam valve coefficient
c_m	Specific heat of metal U-tubes in steam generator
c_{pi}	Specific heat of feedwater in steam generator
F	Fraction of the total power produced in the reactor fuel
h_f	Enthalpy of saturated water
h_g	Enthalpy of saturated steam
h_{fg}	h_f - h_g
m_c	Mass of primary coolant in the core region
$m_{c\text{-}LP}$	Mass of primary coolant in reactor lower plenum
$m_{c\text{-}UP}$	Mass of primary coolant in reactor upper plenum
m_f	Mass of the reactor fuel
m_{m1}	Mass of metal U-tube lump 1
m_{m2}	Mass of metal U-tube lump 2

m_{p1} Mass of coolant in primary coolant lump 1
m_{p2} Mass of coolant in primary coolant lump 2
m_{sw} Mass of water in steam generator
m_{ss} Mass of steam in steam generator
P Thermal power of the reactor core
P_o Initial steady state of reactor thermal power
P_s Steam pressure
P_{so} Initial steady state of steam pressure
S_{ms1} Heat transfer area between steam generator tube metal lump 1 and secondary coolant
S_{ms2} Heat transfer area between steam generator tube metal lump 2 and secondary coolant
S_{pm1} Heat transfer area between primary coolant lump 1 and metal tube lump 1
S_{pm2} Heat transfer area between primary coolant lump 2 and metal tube lump 2
T_{C1} Primary coolant temperature at node 1
T_{C2} Primary coolant temperature at node 2
T_{CL} Primary coolant temperature in cold-leg
T_F Average fuel temperature
T_{fi} Feedwater temperature in steam generator
T_{HL} Primary coolant temperature in hot-leg
T_{IP} Primary coolant temperature in the steam generator inlet plenum
T_{LP} Primary coolant temperature in reactor lower plenum
T_{M1} Average temperature of metal tube lump 1
T_{M2} Average temperature of metal tube lump 2
T_{OP} Primary coolant temperature in the steam generator outlet plenum
T_{P1} Bulk mean temperature of primary coolant lump 1
T_{P2} Bulk mean temperature of primary coolant lump 2
T_{UP} Primary coolant temperature in reactor upper plenum
U_{FC} Heat transfer coefficient from fuel to coolant
U_{ms} Heat transfer coefficient between steam generator tube metal and secondary coolant
U_{pm} Heat transfer coefficient between primary coolant and tube metal in steam generator
v_f Specific volume of saturated water
v_g Specific volume of saturated steam
v_{fg} v_f - v_g
w_c Primary coolant mass flow rate of inside the core
w_{so} Steam flow rate
α_c Coolant temperature coefficient of reactivity
α_F Fuel temperature coefficient of reactivity
β Total delayed neutron fraction
β_i Delayed neutron fraction for the six delayed-neutron groups, $i = 1,\ldots\ldots,6$
Δ Deviation in the dynamic parameters from the steady state
$\delta h_f/\delta P$ Change of enthalpy of saturated water versus steam pressure
$\delta h_g/\delta P$ Change of enthalpy of saturated steam versus steam pressure
$\delta T_{SAT}/\delta P$ Slope of the change in saturation temperature with respect to steam pressure
$\delta v_g/\delta P$ Change in specific volume of saturated steam versus pressure
λ_i Delayed neutron precursor decay constant for the six-delayed neutron group, $i = 1,\ldots\ldots,6$
ρ Reactivity
ρ_{ext} Reactivity induced by control rods
τ_{CL} Coolant residence time in cold-leg
τ_{HL} Coolant residence time in hot-leg
τ_{IP} Coolant residence time in steam generator inlet plenum
τ_{LP} Coolant residence time in reactor lower plenum
τ_{OP} Coolant residence time in steam generator outlet plenum
τ_{P1} Residence time for primary coolant lump 1
τ_{P2} Residence time for primary coolant lump 2
τ_{MP1} $m_{m1}\, c_m/U_{pm}\, S_{pm1}$ = Time constant for metal tube lump 1 to primary coolant lump 1 heat transfer
τ_{MP2} $m_{m2}\, c_m/U_{pm}\, S_{pm2}$ = Time constant for metal tube lump 2 to primary coolant lump 2 heat transfer
τ_{MS1} $m_{m1}\, c_m/U_{ms}\, S_{ms1}$ = Time constant for metal tube lump 1 to secondary coolant heat transfer
τ_{MS2} $m_{m2}\, c_m/U_{ms}\, S_{ms2}$ = Time constant for metal tube lump 2 to secondary coolant heat transfer
τ_{PM1} $m_{p1}\, c_c/U_{pm}\, S_{pm1}$ = Time constant for primary coolant lump 1 to metal tube lump 1 heat transfer
τ_{PM2} $m_{p2}\, c_c/U_{pm}\, S_{pm2}$ = Time constant for primary coolant lump 2 to metal tube lump 2 heat transfer
τ_{UP} $m_{c\text{-}UP}/w_c$ = Coolant residence time in reactor upper plenum; and
Λ Neutron generation time.

Appendix A. Supplementary data

Supplementary data to this article can be found online at https://doi.org/10.1016/j.net.2019.04.017.

References

[1] IAEA, Nuclear Power and Sustainable Development, 2016. http://www.aben.com.br/Arquivos/477/477.pdf%5Cnhttp://jia.sipa.columbia.edu.
[2] World Nuclear Association, Nuclear Power in the World Today, 2019. http://www.world-nuclear.org/information-library/current-and-future-generation/nuclear-power-in-the-world-today.aspx.
[3] J. Barrett, The Canadian Nuclear FactBook, Canadian Nuclear Association, 2017. https://cna.ca/wp-content/uploads/2017/01/2017-Factbook-EN-WEB-FINAL.pdf.
[4] V. Hassija, C. Senthil Kumar, K. Velusamy, Probabilistic safety assessment of multi-unit nuclear power plant sites - an integrated approach, J. Loss Prev. Process. Ind. 32 (2014) 52–62, https://doi.org/10.1016/j.jlp.2014.07.013.
[5] G. Pescaroli, D. Alexander, A definition of cascading disasters and cascading effects : going beyond the " toppling dominos " metaphor, in: GRF Davos Planet@Risk, the 5th IDRC Davos 2014, 2015, pp. 58–67.
[6] R.G. Little, Controlling cascading failure: understanding the vulnerabilities of interconnected infrastructures, J. Urban Technol. 9 (2002) 109–123, https://doi.org/10.1080/106307302317379855.
[7] A. Mosleh, PRA: a Perspective on strengths, current limitations, and possible improvements, Nucl. Eng. Technol. 46 (2014) 1–10, https://doi.org/10.5516/NET.03.2014.700.
[8] C. Perrow, Fukushima and the inevitability of accidents, Bull. At. Sci. 67 (2011) 44–52, https://doi.org/10.1177/0096340211426395.
[9] M. Chino, H. Nakayama, H. Nagai, H. Terada, G. Katata, H. Yamazawa, Preliminary estimation of release amounts of 131 I and 137 Cs accidentally discharged from the Fukushima Daiichi nuclear power plant into the atmosphere, J. Nucl. Sci. Technol. 48 (2011) 1129–1134, https://doi.org/10.1080/18811248.2011.9711799.
[10] M. Holt, R.J. Campbell, M.B. Nikitin, Fukushima Nuclear Disaster (2012), https://doi.org/10.1016/B978-0-12-416727-8.00009-6.
[11] ASME, Forging a New Nuclear Safety Construct, the ASME Presidential Task Force on Response to Japan Nuclear Power Plant Events, 2012. https://www.ipen.br/biblioteca/slr/cel/0087.
[12] IAEA, Deterministic Safety Analysis for Nuclear Power Plants, International Atomic Energy Agency, 2009. https://www-pub.iaea.org/MTCD/publications/PDF/Pub1428_web.pdf.
[13] K.M. Dawson, Advanced Thermal Hydraulic Simulations for Human Reliability Assessment of Nuclear Power Plants by, Massachusetts Institute of Technology, 2017. http://hdl.handle.net/1721.1/112392.
[14] CNSC, Probabilistic Safety Assessment: A Tool to Estimate Risk and Drive Safety Improvement at Nuclear Power Plants, 2017, pp. 1–3. http://nuclearsafety.gc.ca/eng/resources/educational-resources/feature-articles/probabilistic-safety-assessment.cfm.
[15] NUREG/CR-2300, PRA ROCEDURES GUIDE "A Guide to the Performance of Probabilistic Risk Assessments for Nuclear Power Plants,", 1983. https://www.nrc.gov/docs/ML0635/ML063560439.pdf.
[16] R. Bartel, WASH-1400: the Reactor Safety Study. The Introduction of Risk Assessment to the Regulation of Nuclear Reactors, U.S.NRC, 2016.
[17] P. Moieni, A.J. Spurgin, Advances in human reliability analysis methodology. Part I : frameworks, models and data, Reliab. Eng. Syst. Saf. 44 (1994) 27–55.

https://doi.org/10.1016/0951-8320(94)90105-8.
[18] D. Mandelli, C. Parisi, A. Alfonsi, Dynamic PRA of a Multi-Unit Plant, vol. 1, 2017, pp. 1–5. http://www.diegomandelli.com/papers/2017/multiUnitMandelliPSA17_final2.pdf.
[19] S.H. Nejad-Hosseinian, Automatic Generation of Generalized Event Sequence Diagrams for Guiding Simulation Based Dynamic Probabilistic Risk Assessment of Complex Systems, PhD thesis, University of Maryland, 2007.
[20] T. Aldemir, Advanced Concepts in Nuclear Energy Risk Assessment and Management, 2018. https://doi.org/10.1142/10587.
[21] D. Manselli, C. Smith, C. Rabiti, A. Alfonsi, R. Youngblood, V. Pascucci, B. Wang, D. Maljovec, P.T. Bremer, T. Aldemir, A. Yilmaz, D. Zamalieva, Dynamic PRA : an overview of new algorithms to generate, analyze and visualize data, in: Trans. Am. Nucl. Soc, 2013.
[22] A. Amendola, Accident sequence dynamic simulation versus event trees, Reliab. Eng. Syst. Saf. 22 (1988) 3–25, https://doi.org/10.1016/0951-8320(88)90065-8.
[23] C. Acosta, N. Siu, Dynamic event trees in accident sequence analysis: application to steam generator tube rupture, Reliab. Eng. Syst. Saf. 41 (1993) 135–154, https://doi.org/10.1016/0951-8320(93)90027-V.
[24] K.S. Hsueh, A. Mosleh, The development and application of the accident dynamic simulator for dynamic probabilistic risk assessment of nuclear power plants, Reliab. Eng. Syst. Saf. 52 (1996) 297–314, https://doi.org/10.1016/0951-8320(95)00140-9.
[25] K. Coyne, A. Mosleh, Nuclear plant control room operator modeling within the ADS-IDAC, Version 2, Dynamic PRA Environment: Part 1 - general description and cognitive foundations, Int. J. Perform. Eng. 10 (2014) 691–703.
[26] E. Hofer, M. Kloos, B. Krzykacz-Hausmann, J. Peschke, M. Woltereck, An approximate epistemic uncertainty analysis approach in the presence of epistemic and aleatory uncertainties, Reliab. Eng. Syst. Saf. 77 (2002) 229–238, https://doi.org/10.1016/S0951-8320(02)00056-X.
[27] U. Catalyurek, B. Rutt, K. Metzroth, A. Hakobyan, T. Aldemir, R. Denning, S. Dunagan, D. Kunsman, Development of a code-agnostic computational infrastructure for the dynamic generation of accident progression event trees, Reliab. Eng. Syst. Saf. 95 (2010) 278–294, https://doi.org/10.1016/j.ress.2009.10.008.
[28] A. Alfonsi, C. Rabiti, D. Mandelli, J.J. Cogliati, R.A. Kinoshita, A. Naviglio, Dynamic event tree analysis through RAVEN, in: Int. Top. Meet. Probabilistic Saf. Assess. Anal. ANS PSA 2013, 2013, https://doi.org/10.1021/ic302386u.
[29] N.R.C. Job, W. Code, RELAP5/MOD3 Code Manual, vol. 5, 1995.
[30] R.-O. Gauntt, R. Cole, C.M. Erickson, R.G. Gido, R.D. Gasser, S.B. Rodriguez, M.F. Young, MELCOR Computer Code Manuals, 2000.
[31] M. Sonnessa, Modelling and Simulation of Complex Systems, PhD thesis, University of Turin, 2004.
[32] J. Sterman, Business Dynamics: Systems Thinking and Modeling for a Complex World, Irwin Professional/_McGraw–Hill, New York, 2000, https://doi.org/10.1108/13673270210417646.
[33] B.K. Bala, F.M. Arshad, K.M. Noh, System Dynamics: Modelling and Simulation, 2017, https://doi.org/10.1007/SpringerReference_7284.
[34] I. Grigoryev, AnyLogic 7 in Three Days, 2016, https://doi.org/10.1007/s007690000247.
[35] J. Forrester, Some Basic Concepts in System Dynamics, Sloan School of Management. Massachusetts Institute of Technology, 2009. http://www.systemsmodelbook.org/uploadedfile/238_63f73156-02df-4d87-b0c6-c286a7beec26_SomeBasicConcepts.pdf.
[36] A. Borshchev, A. Filippov, From System Dynamics and Discrete Event to Practical Agent Based Modeling: Reasons, Techniques, Tools, Simulation, vol. 66, 2004, pp. 25–29. http://www.econ.iastate.edu/tesfatsi/systemdyndiscreteeventabmcompared.borshchevfilippov04.pdf.
[37] A.M. Yacout, J.J. Jacobson, G.E. Matthern, S.J. Piet, A. Moisseytsev, Modeling the nuclear fuel cycle, in: 23rd Int. Conf. Syst. Dyn. Soc, 2005.
[38] C.J. Jeong, H. Choi, Dynamic modeling and analysis of alternative fuel cycle scenarios in Korea, Nucl. Eng. Technol. 39 (1) (2007).
[39] E.S. Chia, C.K. Lim, A. Ng, N.H.L. Nguyen, The system dynamics of nuclear energy in Singapore, Int. J. Green Energy 12 (2015) 73–86, https://doi.org/10.1080/15435075.2014.889001.
[40] X. Guo, X. Guo, Nuclear power development in China after the restart of new nuclear construction and approval: a system dynamics analysis, Renew. Sustain. Energy Rev. 57 (2016) 999–1007, https://doi.org/10.1016/j.rser.2015.12.190.
[41] Thakkar, Correlation of Theory and Experiment for the Dynamics of a Pressurized Water Reactor, University of Tennessee, 1975. https://trace.tennessee.edu/utk_gradthes/2696%0A%0A.
[42] T.W. Kerlin, E.M. Katz, J.G. Thakkar, J.E. Strange, Theoretical and experimental dynamic analysis of the HB Robinson nuclear plant, Nucl. Technol. 30 (1976) 299–316, https://doi.org/10.13182/NT76-A31645.
[43] M. Ali, Lumped Parameter, State Variable Dynamic Models for U-Tube Recirculation Type Nuclear Steam Generators, PhD thesis, University of Tennessee, 1976, https://trace.tennessee.edu/utk_graddiss/2548%0A%0A.
[44] S. Arda, K.E. Holbert, J. Undrill, Development of a linearized model of a pressurized water reactor generating station for power system dynamic simulations, in: 45th North Am. Power Symp. NAPS 2013, 2013, https://doi.org/10.1109/NAPS.2013.6666832.
[45] S. Arda, Implementing a Nuclear Power Plant Model for Evaluating Load-Following Capability on a Small Grid, MASc Thesis, Arizona State University, 2013.
[46] B. Puchalski, T.A. Rutkowski, K. Duzinkiewicz, Nodal models of Pressurized Water Reactor core for control purposes – a comparison study, Nucl. Eng. Des. 322 (2017) 444–463, https://doi.org/10.1016/j.nucengdes.2017.07.005.
[47] J. Duderstadt, L. Hamilton, Nuclear Reactor Analysis, Department of Nuclear Engineering. The University of Michigan, 1976. http://www.osti.gov/energycitations/product.biblio.jsp?osti_id=7355364.
[48] T. Kerlin, Dynamic Analysis and Control of Pressurized Water Reactors, 1978, pp. 103–212.